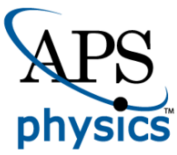

Porosity effects in laminar fluid flow near permeable surfaces

Changwoo Kang and Parisa Mirbod

Phys. Rev. E **100**, 013109 — Published 22 July 2019

DOI: 10.1103/PhysRevE.100.013109

Porosity effects in laminar fluid flow near permeable surfaces

Changwoo Kang and Parisa Mirbod [a)]

Department of Mechanical and Industrial Engineering, University of Illinois at Chicago,

842 W. Taylor Street, Chicago, Il 60607, USA

Abstract

This work analyzes the porosity effects on laminar flow and drag reduction of Newtonian fluids flowing over and through permeable surfaces. A fully-developed laminar flow in a channel partially replaced with a porous material is considered. The analytical solutions for the velocity and shear stress are given and examined to identify the influence of the porosity on the flow. The scaling laws in the porous media are determined using asymptotic analysis in the limit of infinitely small permeability. Direct numerical simulations (DNS) are performed and the transport equation for the kinetic energy is examined to establish the dependency of the porosity on the flow. We found that the impact of the porosity depends on the permeability. For high permeability, the higher porosity induces the increase of driving force and accelerates the flow while it decelerates the flow for low permeability by causing stronger viscous drag of the porous medium.

Key words: Porosity, Permeable/Porous media, Laminar flow, Drag reduction

[a)] Email address for correspondence: pmirbod@uic.edu

Introduction

The flow phenomena over and through porous media have attracted significant interest for decades due to its applicability in a wide range of industrial and environmental applications such as oil and gas reservoirs, thermal insulation, filtration and drying processes, ground-water hydrology, to name a few. It has also been utilized as transport methods for medical and biological applications, including transport in human tissues, bio-convection in biological media, blood flow in microvessels, flow through polymer brushes and chains. Hence, many studies have been attempted to characterize the flow over and through porous media both theoretically and experimentally.

The majority of investigations has focused on predicting the proper formulation at the interface between the free fluid and porous regions. At first, the flow through porous media has been established empirically by Darcy's law (i.e., $Q = -K\nabla p/\mu$) [1], where Q is a volume flow rate per unit area and K is the permeability of the material. However, using this law the velocity changes sharply at the interface between the porous medium and the free fluid layers. To overcome this discontinuity, Beavers and Joseph [2] assumed that the velocity at the interface (i.e., slip velocity) is proportional to the shear rate at the boundary and proposed a relationship between the shear rate and the slip velocity u_s, as

$$\left.\frac{du}{dy}\right|_{y=0} = \frac{\alpha}{\sqrt{K}}(u_s - u_d) \tag{1}$$

where α is a slip coefficient and $u_d = -K\nabla p/\mu$, is the superficial velocity in the porous medium. They validated this boundary condition experimentally in a Poiseuille flow with a permeable wall at the bottom. They showed that the dimensionless quantity α depends on the material parameters which characterize the structure of permeable material within the boundary region [2]. The values of α between 0.1 and 4 showed reasonable agreement with their experimental results. Thereafter, several studies [3-6] were performed to determine the slip coefficient α and revealed that the parameter is strongly dependent on the structure of the boundary and the porous material as well as the working fluid.

A second approach to the problem was introduced by Brinkman [7] who combined Darcy's law and Stokes equation to replace Darcy's law with an equation of higher order given by

$$0 = -\nabla p + \mu_e \nabla^2 \mathbf{u} - \frac{\mu}{K}\mathbf{u} \tag{2}$$

Here, $\mathbf{u}$ is the filtration velocity vector and μ_e is the effective viscosity that may depend on the

geometry of the porous medium and the flow conditions. This equation satisfies the continuity of both velocity and shear stresses, because the Stokes and Brinkman equations are of the same order. The solution of Eq. (2) for the one-dimensional Poiseuille flow was given by Gupte and Advani [8] as

$$u = u_d + (u_s - u_d) \exp\left[\frac{y}{\sqrt{K(\mu_e/\mu)}}\right] \tag{3}$$

This relation obtained by assuming that the porous medium is very thick which can neglect the effect of the lower solid wall of the porous medium (i.e., $u \rightarrow u_d$ as $y \rightarrow -\infty$ and $u = u_s$ at $y = 0$). Differentiating Eq. (3) with respect to y and evaluating it at $y = 0$, the shear rate can be expressed as [8]

$$\left.\frac{du}{dy}\right|_{y=0} = \frac{1}{\sqrt{K(\mu_e/\mu)}}(u_s - u_d) \tag{4}$$

This solution represents that the slip coefficient α in Eq. (1) can be defined as $(\mu/\mu_e)^{1/2}$. This has been used together with Eq. (1) to evaluate α and μ_e by comparing with velocity profiles of experiments [8, 9]. For decades, the Brinkman equation has been extensively employed to examine the flow over and through a porous medium [10-17]. However, it has been shown that the equation is valid only if porosity is high and the effective viscosity μ_e also depends on the structure of the porous material [18].

Meanwhile, the analytical solution of the velocity in the porous and fluid regions to describe flow phenomena which rises from the presence of the permeable wall, for a plane Poiseuille flow using the Brinkman equation, has been given with different forms. Vafai and Kim [14] presented an exact solution for the first time for a classical problem which is a fully-developed flow over a flat plate bounded by a porous medium. They investigated the effects of the Darcy number *Da*, which indicates the dimensionless permeability, and inertia in the porous medium. They revealed that decreasing the permeability results in a lower mass flow rate through the porous region whereas it leads to the increase of the velocity distribution in the free fluid region. The authors also found that higher values of inertia lead to higher velocities in the fluid region because it causes more resistance to the flow of the porous layer; therefore, a larger portion of the mass flow rate has to pass through the fluid layer. Goyeau et al. [18] determined the analytical solution with continuity boundary conditions for velocity and shear stress at the fluid-porous interface. They also compared the thickness of the porous boundary layer and the variation in mass flow rate to their numerical solutions computed in the single-domain as well as previous experiments [2], showing good agreements. Recently,

Mirbod et al. [19] conducted the analytical study for the flow over and through the porous medium in a fully-developed channel. They defined the exact solution for the velocity profile and examined the influences of the permeability and the thickness ratio between the fluid and porous layers on the velocity distribution and drag reduction induced by the permeable wall. The results showed that the permeable wall causes the flow drag reduction and it depends on the permeability and the thickness ratio. As stated above, the Brinkman equation has accounted for the flow and shown good agreements with experimental predictions for a high-porosity medium. To the best of our knowledge, while most of the studies have focused only on the impact of the permeability and the height of a porous medium on flow phenomena, the effect of the porosity of a porous medium, which should be considered for a dense porous [15, 16], still remain unknown.

In this study, we aim to determine the exact solution of the velocity profiles given with the distribution of the shear stress in the fluid and porous layers. The profiles of the velocity and the shear stress are illustrated for various parameters of the permeability and the thickness ratio to analyze the dependency of the porosity on the flow. The effect of both thin and thick porous layer is also examined. The flow drag reduction induced by a porous surface is evaluated by estimating the skin friction at the fluid-porous interface. To validate the analysis, we carry out direct numerical simulations (DNS). To better understand the impact of porosity, we also investigate the kinetic energy variation for flow over and through porous media and the fractional increase in the mass flow rate in the channel. To the best of the authors' knowledge, these are the very first analyses related to exploring the porosity impact in a channel where the lower wall filled with porous media.

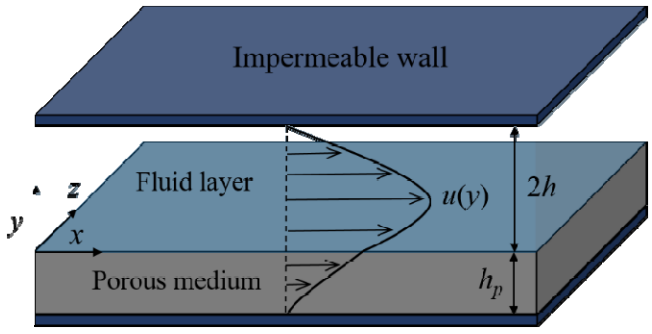

Figure 1. Schematic diagram of a fully developed laminar flow in a rectangular channel over a permeable surface with permeability K and porosity ε, and thickness h_p. Arrows indicate the flow direction and a sketch of the velocity profile.

Theoretical solutions

We consider a fully-developed laminar flow of an incompressible viscous fluid in a channel where its substrate is replaced with a porous medium (Fig. 1). The flow is driven by a constant mean pressure gradient (dp/dx) in the x-direction. A fluid layer with the height $2h$ is bounded by an upper impermeable wall and a permeable wall of porous material, while a porous layer has the thickness h_p and the lower side is sealed by an impermeable wall. We assume the porous medium is saturated by the same fluid and it is homogeneous and isotropic; therefore, porosity ε (i.e., the volume fraction of the fluid in a material) and permeability K of the porous medium are constant.

The governing equations in the fluid layer are the unsteady incompressible continuity and Navier-Stokes equations given by

$$\nabla \cdot \mathbf{u} = 0, \tag{5}$$

$$\rho\left(\frac{\partial \mathbf{u}}{\partial t} + \nabla \cdot (\mathbf{u}\mathbf{u})\right) = -\nabla p + \mu \nabla^2 \mathbf{u}, \tag{6}$$

where $\mathbf{u}$ is the velocity vector (u, v) and p is the pressure, ρ and μ are the density and viscosity of the fluid, respectively. For the flow in the porous layer, the volume-averaged Navier-Stokes (VANS) equations [20, 21] can be stated as

$$\nabla \cdot \langle \mathbf{u} \rangle^s = 0, \tag{7}$$

$$\rho\left(\frac{\partial \langle \mathbf{u} \rangle^s}{\partial t} + \nabla \cdot \left(\frac{\langle \mathbf{u} \rangle^s \langle \mathbf{u} \rangle^s}{\varepsilon}\right)\right) = -\varepsilon \nabla \langle p \rangle^f + \mu \nabla^2 \langle \mathbf{u} \rangle^s - \varepsilon \frac{\mu}{K} \langle \mathbf{u} \rangle^s. \tag{8}$$

Here, $\langle \quad \rangle^s$ and $\langle \quad \rangle^f$ denote the *superficial* and *intrinsic* volume averages where the Dupuit-Forchheimer relationship, i.e., $\langle \quad \rangle^s = \varepsilon \langle \quad \rangle^f$ [20, 21], can be used. They are dropped for the sake of convenience from hence. The third term in the right-hand-side of Eq. (8) represents Darcy's law that describes the average of microscopic (pore-level) flow resistance [1, 7].

For a fully-developed flow considered in this study, the governing equations in the laminar regime ($\partial/\partial t = \partial/\partial x = v = 0$) can be simplified from Eq. (8) as

$$\mu\frac{d^2u}{dy^2}-\varepsilon\frac{\mu}{K}u-\varepsilon\frac{dp}{dx}=0,\qquad y\in[-h_p,0] \tag{9}$$

$$\mu\frac{d^2u}{dy^2}-\frac{dp}{dx}=0,\qquad y\in[0,2h] \tag{10}$$

The no-slip condition is employed on impermeable walls at $y = -h_p$ and $y = 2h$, while the continuity of velocity and shear stress [14] is assumed at the fluid-porous interface ($y = 0$) as follows

$$u(y=0^-)=u(y=0^+)=u_s \tag{11}$$

$$\mu\frac{du}{dy}\Big)_{y=0^-}=\mu\frac{du}{dy}\Big)_{y=0^+} \tag{12}$$

Equations (9) and (10) can be non-dimensionalized with both the half-width of the fluid layer h and the velocity $q=-\left(\frac{h^2}{\mu}\right)\frac{dp}{dx}$ as

$$\frac{d^2\tilde{u}}{d\tilde{y}^2}-\varepsilon\sigma^2\tilde{u}+\varepsilon=0,\qquad \tilde{y}\in[-\delta,0] \tag{13}$$

$$\frac{d^2\tilde{u}}{d\tilde{y}^2}+1=0,\qquad \tilde{y}\in[0,2] \tag{14}$$

where $\tilde{u}=u/q$ and $\tilde{y}=y/h$ are the dimensionless velocity and y coordinate system, $\sigma=h/\sqrt{K}$ is the dimensionless permeability parameter, and $\delta=h_p/h$ is the dimensionless thickness ratio. Using the boundary conditions, analytical solutions of the above equations can be given by

$$\tilde{u}(\tilde{y})=\frac{1}{\sigma^2}+C_1e^{\sigma\sqrt{\varepsilon}\tilde{y}}+C_2e^{-\sigma\sqrt{\varepsilon}\tilde{y}},\qquad \tilde{y}\in[-\delta,0] \tag{15}$$

$$\tilde{u}(\tilde{y})=-\frac{\tilde{y}^2}{2}+\left(1-\frac{\tilde{u}_s}{2}\right)\tilde{y}+\tilde{u}_s,\qquad \tilde{y}\in[0,2] \tag{16}$$

where

$$C_{1,2}=\pm\frac{1}{\sigma^2}\frac{(\sigma^2\tilde{u}_s-1)e^{\pm\sigma\sqrt{\varepsilon}\delta}+1}{e^{\sigma\sqrt{\varepsilon}\delta}-e^{-\sigma\sqrt{\varepsilon}\delta}}\quad,\quad \tilde{u}_s=\frac{\sigma\sqrt{\varepsilon}-\sigma\sqrt{\varepsilon}\,\mathrm{sech}\,\sigma\sqrt{\varepsilon}\delta+\sigma^2\tanh\sigma\sqrt{\varepsilon}\delta}{\left(1+\frac{\tanh\sigma\sqrt{\varepsilon}\delta}{2\sigma\sqrt{\varepsilon}}\right)\sigma^3\sqrt{\varepsilon}}. \tag{17}$$

Therefore, the fluid shear stress $\tilde{\tau}(\tilde{y})=d\tilde{u}/d\tilde{y}$, in the fluid and porous layers can be expressed as

$$\tilde{\tau}(\tilde{y})=\sigma\sqrt{\varepsilon}\left(C_1e^{\sigma\sqrt{\varepsilon}\tilde{y}}-C_2e^{-\sigma\sqrt{\varepsilon}\tilde{y}}\right),\qquad \tilde{y}\in[-\delta,0] \tag{18}$$

$$\tilde{\tau}(\tilde{y}) = -\tilde{y} + 1 - \frac{\tilde{u}_s}{2}, \qquad \tilde{y}\in[0, 2] \tag{19}$$

The skin friction coefficient $C_f=2\tau_w/\rho u_b^2$, is obtained by evaluating the shear stress at the fluid-porous interface (i.e., $\tau_w(y=0)$). Here, u_b is the bulk velocity of the flow in the fluid layer, and the dimensionless one is given by $\tilde{u}_b=0.5\int_0^2 \tilde{u}(\tilde{y})d\tilde{y}$. Hence, the skin friction coefficient induced by the presence of the porous medium is represented as $C_f=A/Re$, where $A = 8(1-\tilde{u}_s/2)/\int_0^2 \tilde{u}(\tilde{y})d\tilde{y}$ and Re is the Reynolds number in the free fluid region defined as $Re = 2\rho u_b h/\mu$. Thus, the skin friction formula for laminar flow in a 2D channel with smooth solid walls can be given by $C_{f_s}=12/Re$ [22]. Finally, the laminar drag reduction D_R, for channel flow with a lower porous wall is computed as

$$D_R=\left(1-\frac{C_f}{C_{f_s}}\right)\times 100\,\% = \left(1-\frac{A}{12}\right)\times 100\,\%\,. \tag{20}$$

Scaling laws as an intermediate asymptotic behavior of the system

Furthermore, we determine the asymptotic behavior of the system in the infinite value of σ by considering the reaction of the system in the low permeability limit. In particular, we define a length scale as a classification between thin and thick porous layer using asymptotic analysis. Taking the limitation of σ as it goes to ∞, and by considering $\operatorname{sech}\sigma\sqrt{\varepsilon}\delta \cong 2e^{-\sigma\sqrt{\varepsilon}\delta}$ and $\tanh\sigma\sqrt{\varepsilon}\delta \cong 1$, Eq. (17) leads to the following leading-order terms for $\tilde{u}_s$ and $C_{1,2}$ as

$$\tilde{u}_s \cong \frac{\sqrt{\varepsilon}+\sigma}{\sigma^2\sqrt{\varepsilon}}\,,\ C_1 \cong \frac{1}{\sigma\sqrt{\varepsilon}}\,,\ C_2 \cong -\frac{e^{-\sigma\sqrt{\varepsilon}\delta}}{\sigma^2}\,, \tag{21}$$

By substituting Eq. (21) into Eqs. (15) and (18), the asymptotic solutions of velocity and shear stress in the porous layer with a rescaled variable $y^* = \sigma\tilde{y}/\delta$ are obtained as

$$u^*(y^*) = \sigma\left(\tilde{u}(\delta y^*/\sigma) - \frac{1}{\sigma^2}\right) = \frac{1}{\sqrt{\varepsilon}}e^{\sqrt{\varepsilon}\delta y^*} - \frac{1}{\sigma e^{\sigma\sqrt{\varepsilon}\delta}}e^{-\sqrt{\varepsilon}\delta y^*}, \qquad y^*\in[-\sigma, 0] \tag{22}$$

$$\tau^*(y^*) = \tilde{\tau}(\delta y^*/\sigma) = e^{\sqrt{\varepsilon}\delta y^*} + \frac{\sqrt{\varepsilon}}{\sigma e^{\sigma\sqrt{\varepsilon}\delta}}e^{-\sqrt{\varepsilon}\delta y^*}, \qquad y^*\in[-\sigma, 0] \tag{23}$$

Here, u^* and τ^* represent the rescaled velocity and shear stress. The above solutions show two different limits depending on whether the length scale $\Lambda=\sigma\delta \ll 1$ or $\Lambda \gg 1$. The parameter Λ signifies a specific vertical length scale associated with the porous medium thickness and

its relative permeability. We introduce systems of $\Lambda \ll 1$ and $\Lambda \gg 1$ as thin and thick porous media, respectively, that has also been reported by Battiato [23]. Basically, $\Lambda \ll 1$ indicates a system with a small thickness of a porous medium and $\Lambda \gg 1$ reflects a porous media with a large thickness for constant values of permeability. Therefore, the asymptotic solutions for each case can be defined as

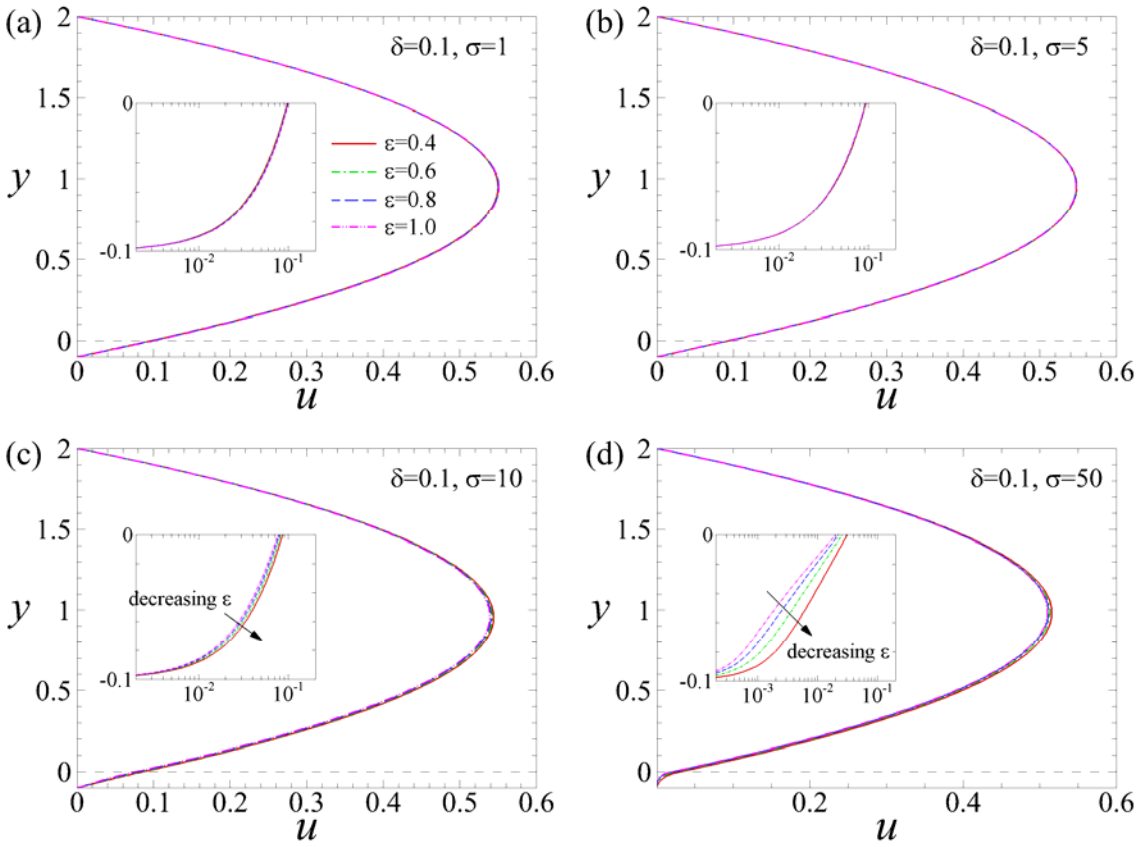

Figure 2. Variations of normalized velocity profile in the fluid and porous layers for δ=0.1. (The dashed line at $y = 0$ indicates the interface of fluid-porous region.)

$$\begin{cases} u^*(y^*) = \dfrac{1}{\sqrt{\varepsilon}} e^{\sqrt{\varepsilon}\delta y^*} - \dfrac{1}{\sigma e^{\sigma\sqrt{\varepsilon}\delta}} e^{-\sqrt{\varepsilon}\delta y^*} \\ \tau^*(y^*) = e^{\sqrt{\varepsilon}\delta y^*} + \dfrac{\sqrt{\varepsilon}}{\sigma e^{\sigma\sqrt{\varepsilon}\delta}} e^{-\sqrt{\varepsilon}\delta y^*} \end{cases}, \quad y^* \in [-\sigma, 0] \quad \text{if} \quad \Lambda \ll 1 \tag{24}$$

$$\begin{cases} u^*(y^*) = \dfrac{1}{\sqrt{\varepsilon}} e^{\sqrt{\varepsilon}\delta y^*} \\ \tau^*(y^*) = e^{\sqrt{\varepsilon}\delta y^*} \end{cases}, \quad y^* \in [-\sigma, 0] \quad \text{if} \quad \Lambda \gg 1 \tag{25}$$

Results and Discussion

In the present study, we consider the porosity in the range of ε = 0.4~1.0 and the thickness ratio δ, varies from 0.1 to 4.0. This range of porosity has been chosen to generalize our analytical study for a various range of porous media. The tildes in the velocity and the shear stress are omitted for the sake of the convenience.

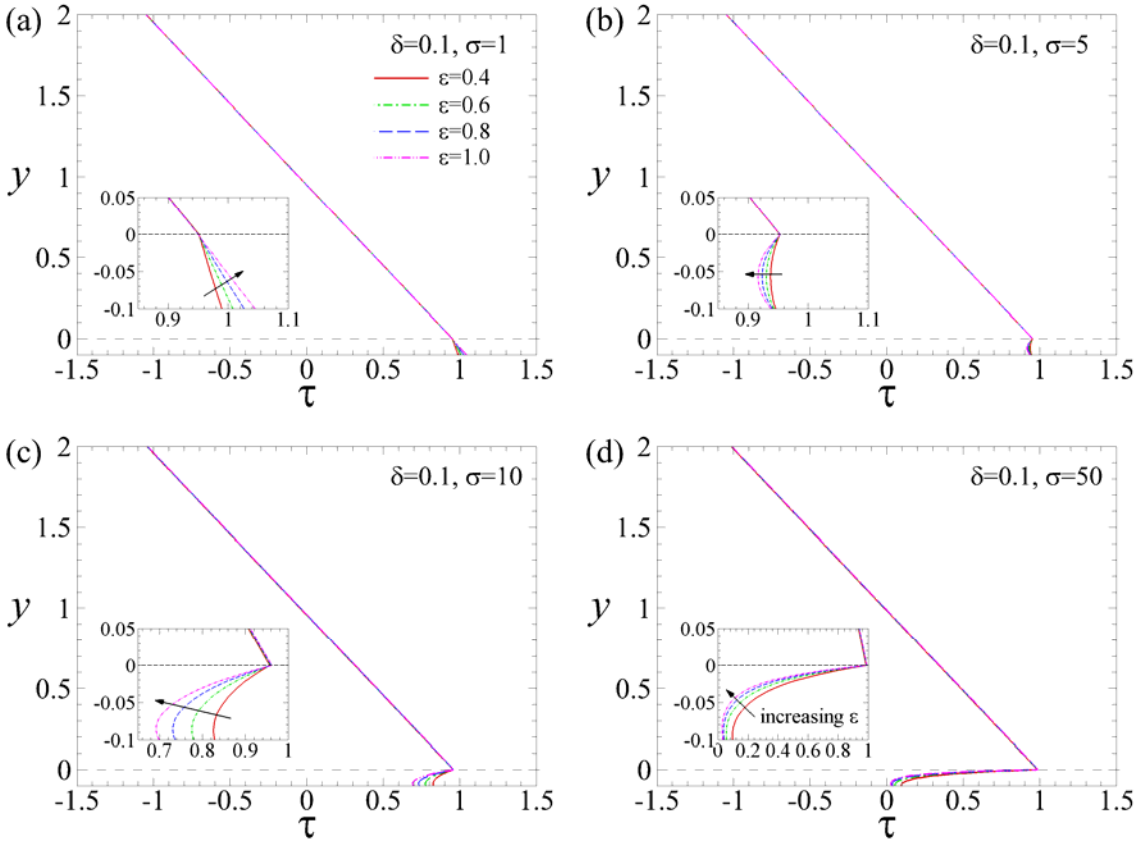

Figure 3. Variations of normalized shear stress profile in the fluid and porous layers for δ=0.1. (The dashed line at y = 0 indicates the interface of fluid-porous region.)

Thin porous layer ($\Lambda \ll 1$)

Figure 2 shows velocity profiles of laminar flow over a very thin porous layer for δ = 0.1. As expected for low σ (i.e., $K \approx \infty$), the porosity does not have a critical effect on the profiles of the fluid (Fig. 2(a), (b)). However, as shown in Fig. 2(c), (d), it causes a noticeable difference on the velocity field for higher σ (i.e., $K \approx \infty$) due to the impact of the porous media. In addition, by increasing both σ and ε, the velocity in the porous medium decays that leads to a decrease in the velocity at the fluid-porous interface u_s. This is because by reducing the pore space accessible to flow in the porous layer as the ability of the porous to transmit the

fluid decays, the fluid flowing inside the porous is accelerated.

As displayed in Fig. 3, the variation of the porosity does not make a remarkable effect on the shear stress $\tau(y)$ in the fluid region while the impact of the porosity in the porous layer appears to be critical. For high permeability (i.e., σ =1), the growing ε only gradually strengthens the shear stress rate (Fig. 3(a)). On the other hand, the shear stress diminishes as the permeability decreases and the increasing ε steadily weakens the shear stress of the fluid near the bottom of the porous medium (Fig. 3(b)-(d)). This is because as the permeability decreases and the space of pore regions in the porous layer increases, the bulk of shear stress is sustained by the solid matrix in the porous layer, which results in very small velocity and fluid shear stress. Note that the solid stress inside the porous media is not assessed in this work.

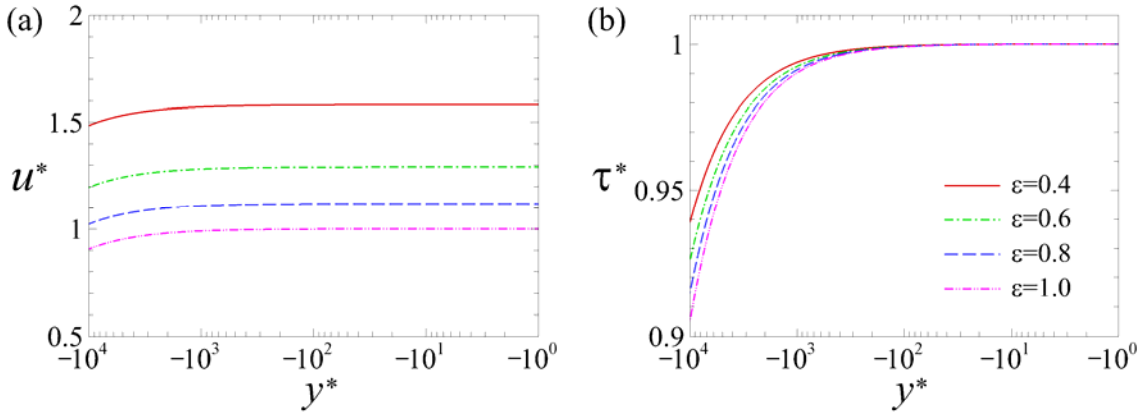

Figure 4. Asymptotic profiles of the rescaled velocity and shear stress inside a thin porous medium ($\Lambda \ll 1$) for $\sigma = 10^4$ and $\delta = 10^{-5}$ where Λ=0.1.

Asymptotic solutions of rescaled velocity and shear stress obtained in Eq. (24) for a thin porous medium (i.e., Λ=0.1) have been plotted in Fig. 4. Fig. 4(a) shows that the rescaled velocity u^* is inversely proportional to $\sqrt{\varepsilon}$. Figure 4(b) reveals that the rescaled shear stress as it approaches to the interface ($y^* \to 0$) becomes constant τ^*=1 regardless of the porosity value. The stress gradually decreases as it goes far away from the interface ($y^* \to -\sigma$), showing its dependency on the porosity. In addition, as ε increases the rescaled velocity and shear stress diminishes inside a thin porous medium. The reason is that as the space in which the fluid moves increases, the flow resistance rises leading to the decay in the ability of the

fluid passing through the porous medium. These results turn out that the pore structure of a porous medium plays a critical role for thin porous layer. The same trend has been identified in profiles of analytical solutions for low permeability as shown in Fig. 2(d) and 3(d).

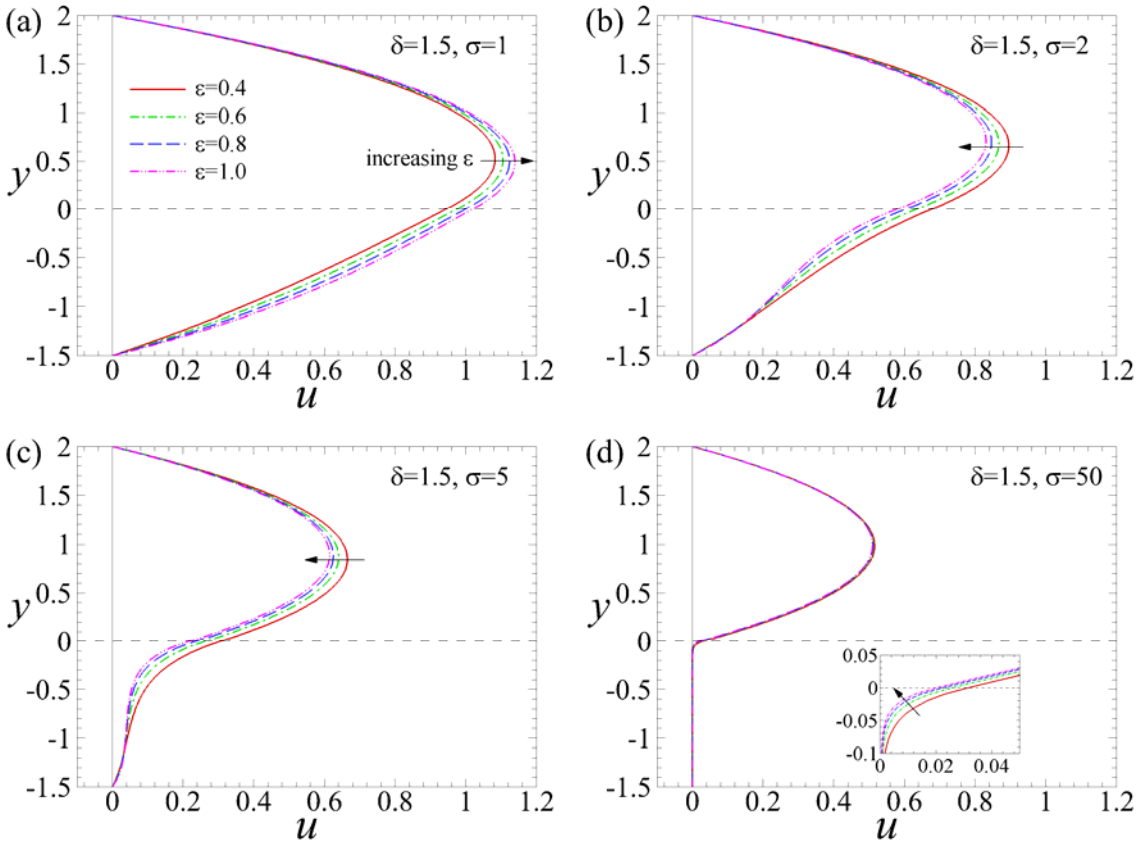

Figure 5. Variations of normalized velocity profile in the fluid and porous layers for δ=1.5. (The dashed line at y = 0 indicates the interface of fluid-porous region.)

Thick porous layer ($\Lambda \gg 1$)

The porosity effect on the velocity profile is significantly different for the flow over a thick porous medium. Velocity profiles for various ε and σ at δ=1.5 are illustrated in Fig. 5. As shown clearly in Fig, 5(a), the velocity gradually grows with increasing ε in both fluid and porous layers for very low σ (i.e. $K \approx \infty$), resulting in the enhancement of the slip velocity u_s. In contrast, increasing porosity and σ leads to the reduction of the velocity as well as u_s (Fig. 5(b), (c)). This is due to the decay in the permeability which preserves the flow inside the porous media. The influence of porosity becomes weak as the permeability of porous media

decays. For very high σ, the velocity in the porous material drops to very small value and the velocity profiles has the characteristics of the plug flow inside the porous layer except for a flow near the interface known as the Brinkman's layer (Fig. 5(d)). Also, the slip velocity u_s diminishes with growing porosity. These results prove the importance of the permeability compared to the porosity of the porous media.

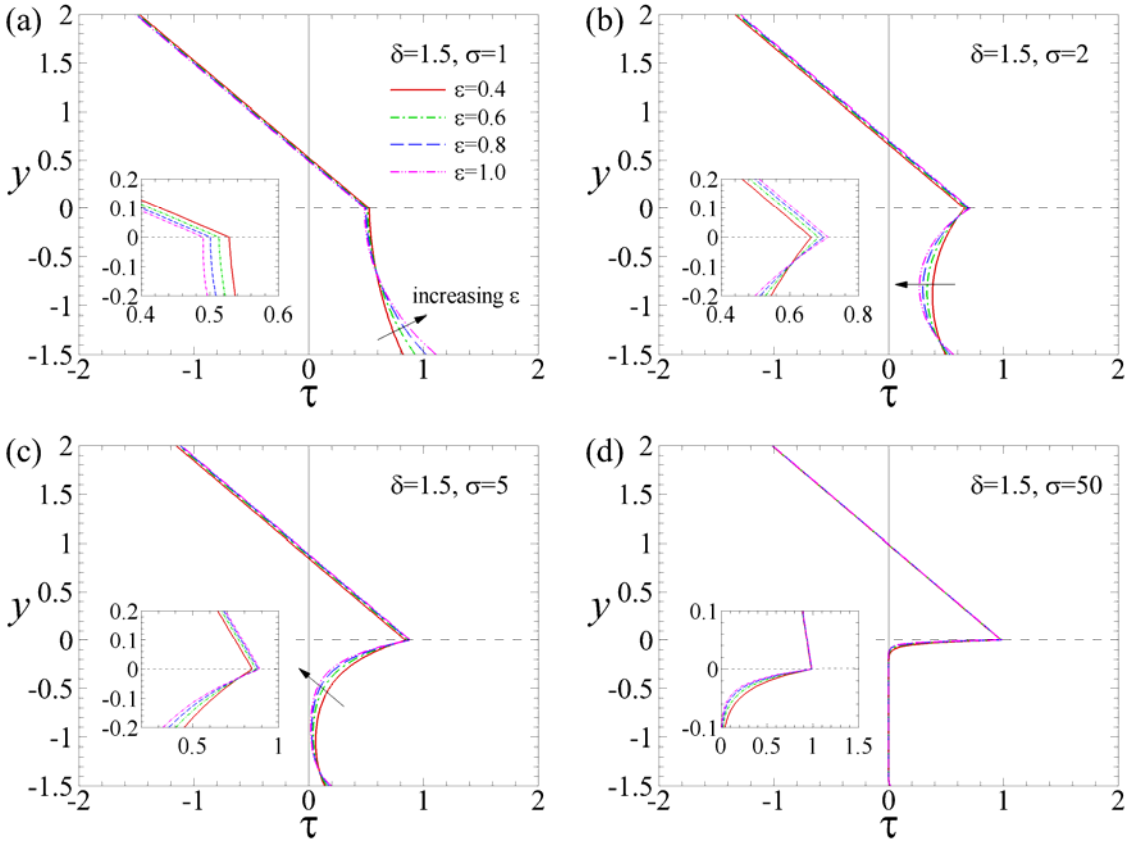

Figure 6. Variations of normalized shear stress profile in the fluid and porous layers for δ=1.5. (The dashed line at y = 0 indicates the interface of fluid-porous region.)

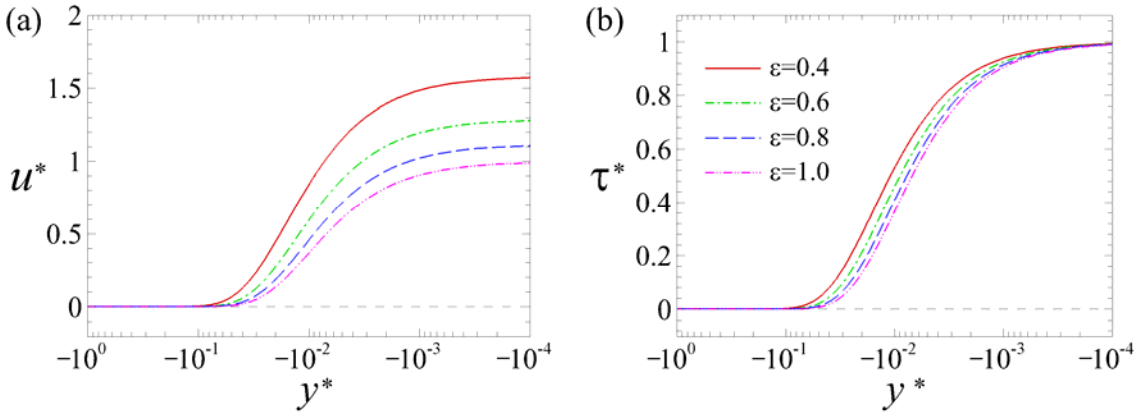

Figure 7. Asymptotic profiles of rescaled velocity and shear stress inside a thick ($\Lambda \gg 1$) porous medium for $\sigma = 10^2$ and $\delta = 10^2$ ($\Lambda = 10^4$).

Profiles of the shear stress $\tau(y)$ for various σ are presented in Fig. 6. The porosity effect is slightly limited in the fluid layer for all σ, while the profiles in the porous layer show the dependency on the porosity. For low σ, as ε rises the shear stress at the interface decays. However, the shear stress near the bottom wall of the porous layer increases (Fig. 6(a)). The shear stress gradually becomes stronger by further increasing σ, and the growing ε reduces the stress of the fluid within the porous medium (Fig. 6(b), (c)). Finally, for very high value of σ, the shear stress approaches to zero inside the porous media (Fig. 6(d)).

Figure 7 displays the asymptotic behavior of the velocity and shear stress defined in Eq. (25) for a thick porous medium (i.e., $\Lambda = 10^4$). The rescaled velocity u^* becomes zero near the bottom of a porous medium ($y^* \rightarrow -\sigma$). However, it steadily increases as it approaches to the interface ($y^* \rightarrow 0$) and it is proportional to $1/\sqrt{\varepsilon}$ in the vicinity of the interface (Fig. 7(a)). The rescaled shear stress τ^* is also 0 as $y^* \rightarrow -\sigma$. It grows increasingly with $y^* \rightarrow 0$, and it converges to a constant value (i.e., $\tau^* = 1$) at the interface as seen in Fig. 7(b). Therefore, the porosity is a key parameter in characterizing the flow for both thin and thick porous media. These agree with the experimental analysis have been performed in our previous work [24].

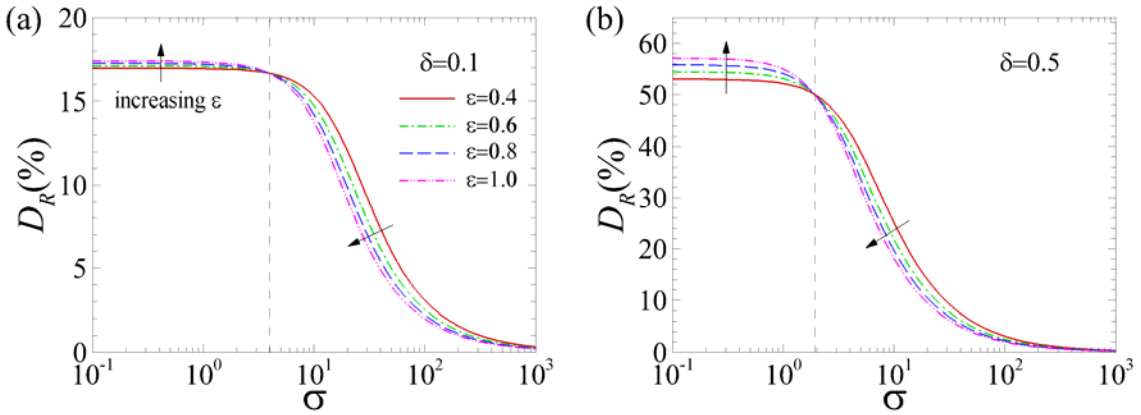

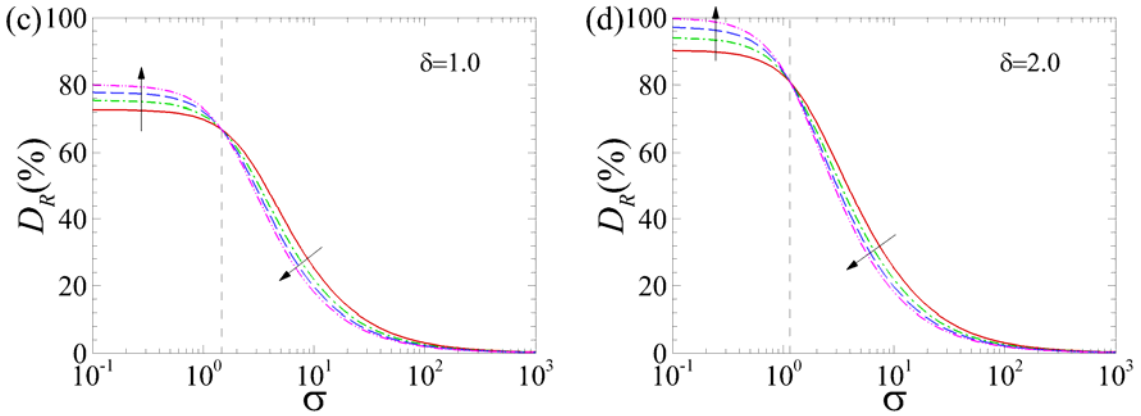

Figure 8. Drag reduction D_R vs. σ for various δ.

Moreover, we have analyzed the drag reduction to examine the behavior of the porosity for laminar flow over porous media. The variation of drag reduction (D_R) with the permeability parameter for various thickness of the porous layer has been plotted in Fig. 8. As can be seen, by thickening the porous medium the drag reduction enhances. The porosity effect on the drag reduction depends on the permeability parameter σ. At low σ, by increasing the porosity the drag reduction is improved. As δ increases, the impact of the porosity could be more pronounced. On the other hand, for all depth ratios δ by increasing porosity as the permeability of the porous layer decreases the drag reduction diminishes. However, as the permeability parameter further increases the drag reduction approaches to 0, which represents that C_f at the interface approaches to the skin friction coefficient of the flow in a smooth channel with solid walls. Thus, the variation of the porosity does not make a difference at very high σ (i.e., $K \approx 0$). In addition, for each δ there is a value of σ at which the drag reduction is independent on the variation of the porosity (indicated as the dashed line). For the intersecting point of σ, the trend of the porosity influence is reversed, i.e., gradually moves to lower values of σ as the porous layer thickens.

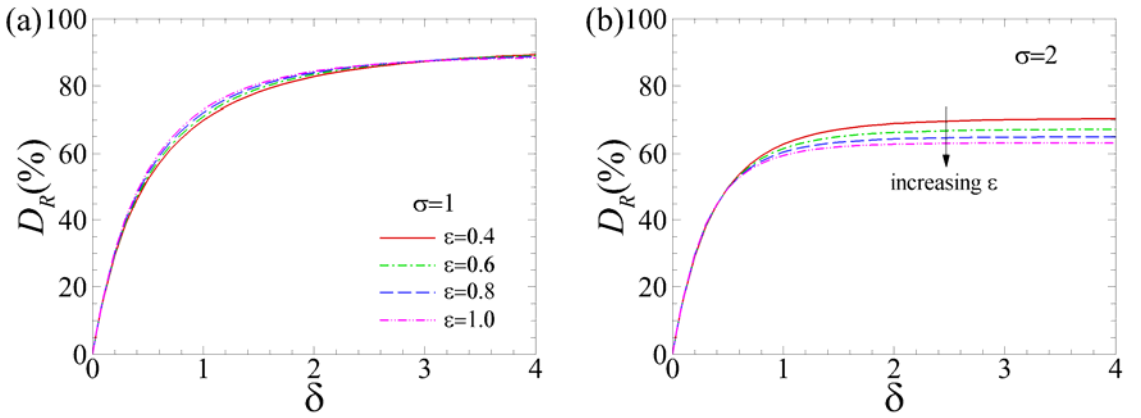

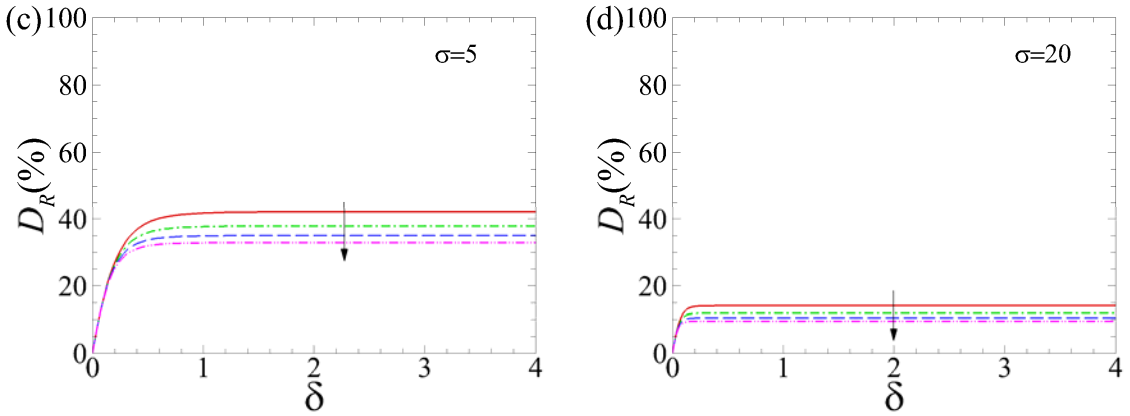

Figure 9. Drag reduction D_R vs. δ for various σ.

Figure 9 shows the drag reduction (D_R) versus the thickness of the porous material δ, for various permeability parameter σ. As mentioned earlier, the higher permeability (i.e., low σ) leads to the more drag reduction. The drag reduction converges to a constant value as the porous layer becomes thicker, and it is reached more rapidly at higher σ. These converged values of D_R depend on σ and ε that show large values at the lower porosity for high σ. Interestingly, even for low values of permeability the drag reduction can be observed in the system in which increasing the porosity results in the growth of the drag reduction.

Mass flow rate Analysis

To understand how a real porous media with specific porosity may affect the flow in a channel, we characterized the fractional increase in the mass flow rate Φ, in the fluid layer with the existence of a permeable wall. Beavers and Joseph [2] introduced the fractional increase of the mass flow rate in the fluid layer due to the presence of the porous medium and compared it with the experiments. Based on the Darcy's Law, it can be expressed as

$$\Phi = \frac{Q_p - Q_i}{Q_i} = \frac{3(\sigma + \alpha)}{\sigma(1 + 2\alpha\sigma)} \tag{26}$$

where Q_p is the mass flow rate in a channel with permeable and impermeable surfaces, and Q_i indicates the mass flow rate with two impermeable walls. Beavers and Joseph [2] used porous blocks of foametals and aloxite for experiments and plotted Φ versus σ. They predicted α= 0.78 ~ 4.0 for foametals and α= 0.1 for aloxite. It appeared these data to be consistent with their experiments for oil and water flows over porous blocks, even though the measured values were considerably scattered.

Using Brinkman equation the fractional increase is also given by [18, 25]

$$\Phi = \frac{3(\sigma + 1/\sqrt{\varepsilon})}{\sigma(1 + 2\sigma/\sqrt{\varepsilon})} \tag{27}$$

Goyeau et al. [18] used the viscosity ratio as $\mu_e/\mu_f = \varepsilon^{-1}$ with $\varepsilon = 0.78$ for comparison. Their prediction showed good agreement with those of Beavers and Joseph [2] for $\alpha = 1.2$ (Fig. 10(a)).

In this study, we determine the fractional increase in mass flow rate by using Eq. (16) as

$$\Phi = \frac{\int_0^2 -\frac{y^2}{2} + \left(1 - \frac{u_s}{2}\right) y + u_s \, dy}{\int_0^2 y\left(1 - \frac{y}{2}\right) dy} - 1 = \frac{3}{2} u_s \tag{28}$$

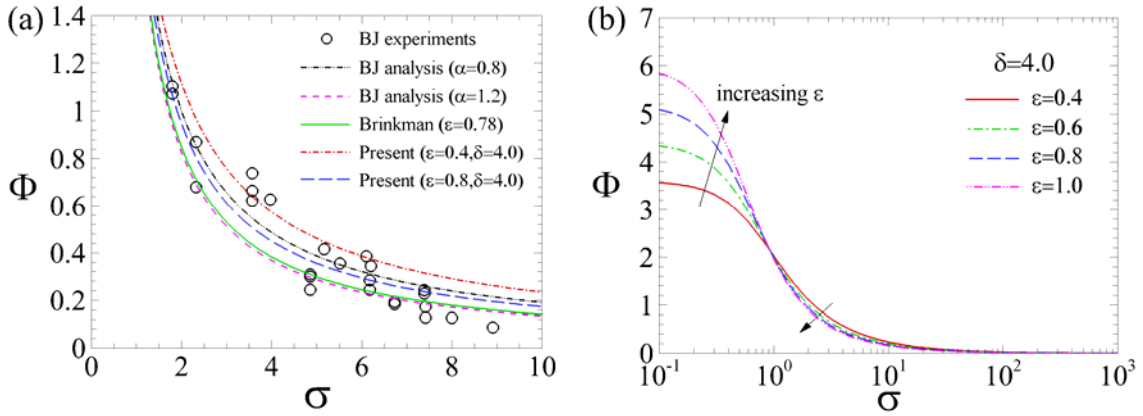

Figure 10. Fractional increase of the mass flow rate (Φ) as a function of σ (BJ: Beavers and Joseph [2]).

Fig. 10(a) shows the plots of $\varepsilon = 0.4$ and $\varepsilon = 0.8$ for $\delta = 4.0$ and various σ. We found that the results for $\varepsilon = 0.8$ are in excellent agreement with the analytical solution of Beavers and Joseph [2] for $\alpha = 0.8$. The curve related to $\varepsilon = 0.4$ is also in-line with their experimental values. Although experimental data were quite scattered, our results are in error bound as the analytical values reported by [2, 18]. It should be noted that the discrepancy in Φ values for $\varepsilon = 0.78$ between this study and the data reported in [18], where both are based on the Brinkman equation, results from the difference of the boundary condition at the bottom wall ($y = -h_p$) of a porous medium. We employed the no-slip boundary condition at the wall as $u(y = -h_p) = 0$, whereas Goyeau et al. [18] used the Darcy's law.

We have also displayed the fractional increase of the mass flow rate Φ, given by Eq. (28) for various porosity and $\delta = 4$ in Fig. 10(b). This figure shows that for small values of σ, as ε

increases, Φ increases, whereas it decreases for higher σ values. The fractional increase gradually diminishes as σ rises, and approaches to zero, which represents the channel flow with an impermeable wall (i.e. solid wall) for very high σ. This is due to the fact that as the permeability and porosity increase, the flow rate in the channel builds up.

Verification using Direct Numerical Simulations (DNS)

In this section, we perform a direct numerical simulation (DNS) by solving the governing equations for two-dimensional incompressible flow to verify the result of analytical solutions and further analyze the characteristics of the flow. For DNS, we introduce the single-domain approach in which the porous layer is treated as a pseudo-fluid and composite region is considered as a continuum [18]. This approach has been extensively employed in numerical simulation for the flow in fluid and porous layers [26-29]. We use the volume-averaged equations Eqs. (7) and (8) for current numerical simulations. In the fluid layer, we consider ε = 1 and the permeability K is infinite. The governing equations were discretized using a finite volume method in a Cartesian grid system. A second-order central difference scheme was utilized for spatial discretization of derivatives. A hybrid scheme was used for time advancement; nonlinear terms were explicitly advanced by a third-order Runge-Kutta scheme, and the other terms were implicitly advanced by the Crank-Nicolson method [30, 31]. A fractional-step method was employed for time integration and the Poisson equation resulted from the second stage of the fractional step method was solved by a fast Fourier transform (FFT) [32].

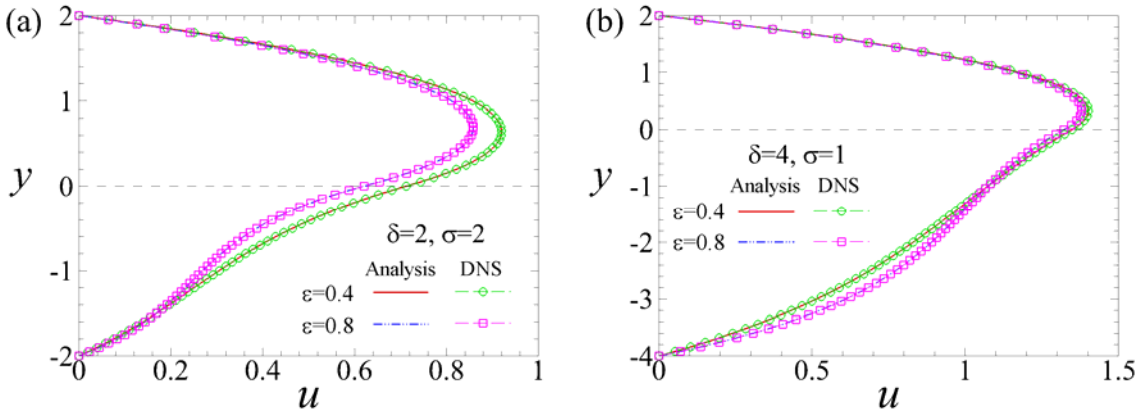

Figure 11. Normalized velocity profiles in the fluid and porous layers for (a) δ = 2, σ = 2 and (b) δ = 4, σ = 1.

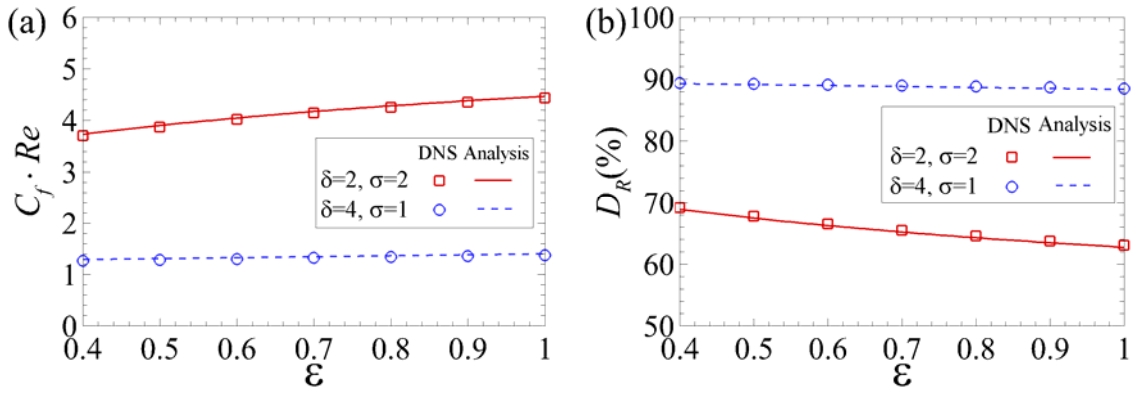

Figure 12. Skin-friction coefficients (C_f) and drag reductions (D_R) for various ε.

Table 1. Comparison of flow parameters between DNS and analytical predictions.

δ	σ	ε	DNS			Analytical results		
			u_s	$u_s/u_{\max}$	$u_s/\dot{\gamma}\sqrt{K}$	u_s	$u_s/u_{\max}$	$u_s/\dot{\gamma}\sqrt{K}$
0.1	1	0.8	0.0988	0.179	0.104	0.0988	0.179	0.104
0.1	10	0.8	0.0796	0.147	0.831	0.0796	0.147	0.831
2	2	0.4	0.713	0.775	2.215	0.713	0.775	2.215
2	2	0.8	0.621	0.723	1.801	0.621	0.723	1.801
4	1	0.4	1.349	0.962	4.147	1.349	0.962	4.147
4	1	0.8	1.322	0.958	3.902	1.322	0.958	3.902
4	50	0.8	2.25×10^{-2}	0.044	1.138	2.25×10^{-2}	0.044	1.138
4	100	0.8	1.12×10^{-2}	0.024	1.224	1.12×10^{-2}	0.024	1.224

The no-slip condition was imposed on impermeable solid walls, and the flow was assumed to be periodic in the streamwise direction x. The velocity and shear stress at the interface were assumed to be continuous (Eqs. (11) and (12)). The number of grid points used in this study is 64(x)×250(y) for δ=0.1, 64(x)×400(y) for δ=2, and 64(x)×600(y) for δ=4 with the axial length of the domain 4h. More grid points are allocated near solid walls and interface between the two layers in the y-direction with $\Delta y_{\min}$= 0.002, whereas the grid cell in the x-direction is uniform.

The computed velocity profiles in two layers for several control parameters are presented in

Fig. 11 with those of analytical solutions (Eqs. (15) and (16)). In addition, the slip velocity u_s and shear stress rate $\dot{\gamma} = \partial u/\partial y|_{y=0}$ at the interface between two layers for the values are compared in Table 1. As can be seen in Fig. 11, the velocity distributions are perfectly aligned with analytical profiles. The obtained values of the velocity and the shear rate at the interface show an excellent agreement with those of theoretical predictions (Table 1). We also have calculated the skin-friction coefficient C_f on the permeable wall and the drag reduction (D_R) for various ε, δ, and σ shown in Fig. 12. Our computed values strongly confirm the predicted analytical solutions.

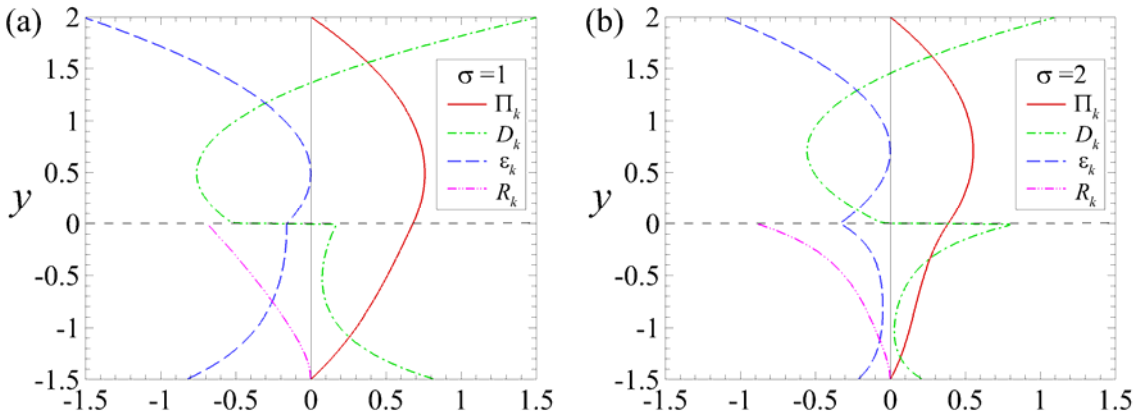

Figure 13. Profiles of different terms of the kinetic energy balance equation for $\delta = 1.5$ and $\varepsilon = 1.0$. The values were normalized by q^3/h.

Variation of the kinetic energy

Next, we investigate the variation of kinetic energy for flow over and through porous media as the porosity and permeability of the porous media vary.

The transport equation for the kinetic energy ($k = u_i u_i/2$) can be derived from the Navier-Stokes equations and in both fluid and porous regions can be stated as

$$\frac{Dk}{Dt} = \underbrace{-\frac{\varepsilon}{\rho}\left(u_i \frac{\partial p}{\partial x_i}\right)}_{\Pi_k} \underbrace{+\nu \frac{\partial^2 k}{\partial x_j{}^2}}_{D_k} \underbrace{-\nu\left(\frac{\partial u_i}{\partial x_j}\frac{\partial u_i}{\partial x_j}\right)}_{\varepsilon_k} \underbrace{-2\varepsilon \frac{\nu}{K} k}_{R_k}, \quad y \in [-h_p, 0] \tag{29}$$

$$\frac{Dk}{Dt} = \underbrace{-\frac{1}{\rho}\left(u_i \frac{\partial p}{\partial x_i}\right)}_{\Pi_k} \underbrace{+\nu \frac{\partial^2 k}{\partial x_j^2}}_{D_k} \underbrace{-\nu\left(\frac{\partial u_i}{\partial x_j}\frac{\partial u_i}{\partial x_j}\right)}_{\varepsilon_k}, \qquad y\in[0,\ 2h] \tag{30}$$

where $\nu = \mu/\rho$ and $D/Dt = \partial/\partial t + u_j \partial/\partial x_j$. This equation composed of the velocity pressure-gradient Π_k, viscous diffusion D_k, and viscous dissipation ε_k terms, and the viscous drag originated from Darcy's Law R_k which indicates the viscous resistance of a porous medium.

The vertical distribution of all terms of the transport equation for the kinetic energy are plotted in Fig. 13. In the fluid layer, the kinetic energy is mainly produced by the pressure gradient Π_k and is vanished by the viscous diffusion D_k, while it is mostly balanced by the viscous diffusion and dissipation ε_k terms near the upper wall (i.e., $y = 2$). Hence, the viscous diffusion term D_k has positive values in the whole porous medium. The term generates the kinetic energy is the pressure gradient Π_k, and the energy is dissipated by the viscous dissipation ε_k and drag R_k terms. The equilibrium of the kinetic energy is maintained by the viscous diffusion D_k and dissipation ε_k terms close to the bottom wall (i.e., $y = $ □1.5). However, the contribution of each term on the variation of the kinetic energy principally depends on the permeability parameter σ. For low σ, the energy is primarily produced by the pressure gradient Π_k and it is vanished by the dissipation and viscous drag (Fig. 13(a)). On the other hand, the viscous drag R_k induced by the porous medium mostly dissipates the kinetic energy in the porous layer and it is balanced by the viscous diffusion D_k near the interface for higher σ (Fig. 13(b)). Accordingly, it could be concluded that the contribution of the pressure gradient is most dominant on the variation rate of the kinetic energy for high permeability (i.e., low σ), whereas the viscous drag term plays an important role in the kinetic energy transport for low permeability.

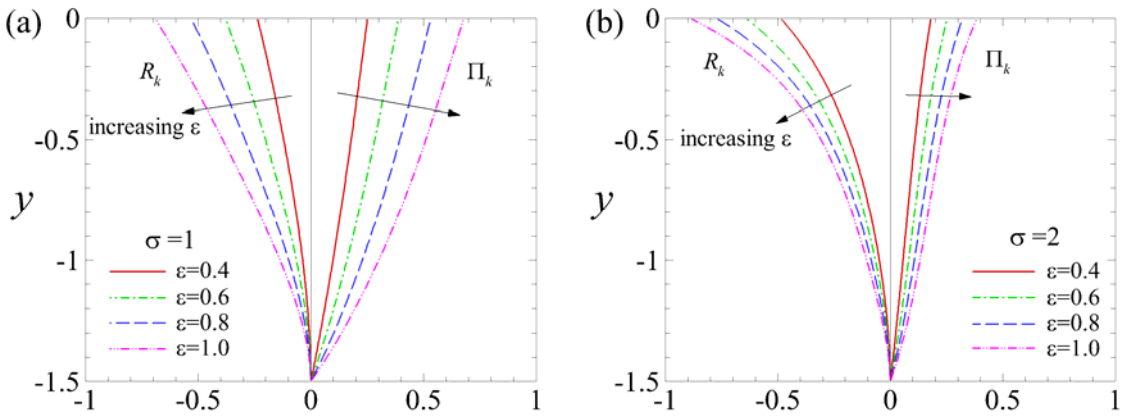

Figure 14. Distributions normalized by q^3/h of the velocity pressure-gradient Π_k (positive

values) and viscous drag R_k (negative values) terms within the porous layer for various ε at δ = 1.5.

Previously, we have shown the dependency of the porosity ε on the velocity profiles in both fluid and porous layers in which by increasing ε the velocity profile for low σ enhances, while the velocity is reduced by the growing ε for high σ (Fig. 5). These could be explained by the analysis of the transport equation for the kinetic energy shown above. Figure 14 illustrates profiles of the velocity pressure-gradient Π_k and viscous drag R_k terms of the transport equation for various ε. As described earlier, the pressure gradient largely contributes to the production of the kinetic energy in the porous layer for low σ. Figure 14(a) reveals that the variation rate of the velocity pressure-gradient Π_k term is amplified with the growth of ε at low σ. Consequently, for high permeability (i.e., low σ) the higher porosity causes the acceleration of the flow in the porous medium by increasing the contribution of the pressure gradient. This leads to the enhancement of the slip velocity at the interface and the mass flow rate in the fluid region. In addition, the viscous drag induced by Darcy's Law has a substantial contribution on the energy dissipation for high σ (Fig. 14(b)). As can be seen in Fig. 14(b), the dissipation rate of the viscous drag R_k is larger than the production rate generated by the pressure gradient Π_k, and the variation rate of R_k steadily grows with the increasing ε. Therefore, it could be deduced that increasing ε results in the deceleration of the flow through the porous layer by enhancing the dissipation rate of the viscous drag in the kinetic energy for the low permeability. This then reduces the slip velocity and the flow rate in the fluid layer.

Conclusion

In this work, we have investigated the effect of the porosity ε of a porous medium on the laminar flow in a channel replaced by a porous layer. The analytical solutions have been obtained from the governing equations in which the volume-averaging approach was employed and the Darcy's Law was used to model the pore-level flow resistance in the porous medium. The solutions have been determined by porosity, permeability K, and the thickness of a porous medium δ, that have also been verified by direct numerical simulations. The influence of the porosity on the velocity in the fluid and porous layers depend on the permeability. The increasing value of the porosity enhances the velocity in both layers for the high permeability (i.e. low σ), while it reduces the flow rate for the low permeability (i.e. high σ). The shear stress at the interface decays with the rising porosity when the permeability is

high, and it leads to the reduction of the skin-friction C_f at the interface and the improvement of the drag reduction D_R. However, the stress rate between two layers becomes stronger with the increase of the porosity for the low permeability, and it results in the increase of the skin-friction at the interface and diminishes the drag reduction.

The self-similar solutions of the flow through a porous medium have been obtained using asymptotic behavior analysis in the infinitely small permeability limit (i.e. $\sigma \to \infty$). The self-similarity reveals two different behaviors that depend on a spatial length scale $\Lambda = \sigma\delta$ related to the thickness of a porous medium. The asymptotic solutions for the velocity and shear stress are classified into those of thin ($\Lambda \ll 1$) and thick ($\Lambda \gg 1$) porous media. The rescaled quantities exhibit the same behaviors with those of analytical solutions for the flow with a very low permeability.

The transport equation of the kinetic energy has been evaluated to explore the effects of the porosity on the velocity in the fluid and porous regions. For high permeability, the flow is accelerated with the growth of the porosity by increasing the driving force of the pressure gradient. Hence, the higher porosity causes the deceleration of the flow for low permeability, since it enhances the viscous drag of the porous medium.

This study provides valuable insights into understanding flow in a channel in the existence of permeable surfaces. It helps scientists and researchers in various disciplines to examine flow transport over and through porous media including canopies [33], porous track, and porous bearings [34-36] as well as heat and fluid flow on rough surfaces [37-39]. Analysis of complex fluids over porous media is the focus of our current study [40, 41].

Acknowledgements

This work has been supported partially by National Science Foundation award#1854376 and partially by Army Research Office award#W911NF-18-1-0356.

References

[1] H. P. G. Darcy, *Les Fontaines Publique de la Ville de Dijon*. Paris: Victor Dalmont (1856).

[2] G. S. Beavers and D. D. Joseph, "Boundary conditions at a naturally permeable wall," *J. Fluid Mech.* **30**, 197-207 (1967).

[3] G. S. Beavers, E. M. Sparrow and R. A. Magnuson, "Experiments on coupled parallel flows in a channel and a bounding porous medium," *J. Basic Eng.* **92**, 843-848 (1970).

[4] G. I. Taylor, "A model for the boundary condition of a porous material. Part 1," *J. Fluid Mech.* **49**, 319-326 (1971).

[5] S. Richardson, "A model for the boundary condition of a porous material. Part 2," *J. Fluid Mech.* **49**, 327-336 (1971).

[6] G. S. Beavers, E. M. Sparrow and B. A. Masha, "Boundary condition at a porous surface which bounds a fluid flow," *AIChE J.* **20**, 596-597 (1974).

[7] H. C. Brinkman, "A calculation of the viscous force exerted by a flowing fluid on a dense swarm of particles," *App. Sci. Res.* **A1**, 27 (1947).

[8] S. K. Gupte and S. G. Advani, "Flow near the permeable boundary of a porous medium: An experimental investigation using LDA," *Exp. Fluids* **22**, 408-422 (1997).

[9] S. Kim and W. B. Russel, "Modelling of porous media by renormalization of the Stokes equations," *J. Fluid Mech.* **154**, 269-286 (1985).

[10] T. S. Lundgren, "Slow flow through stationary random beds and suspensions of spheres," *J. Fluid Mech.* **51**, 273-299 (1972).

[11] D. A. Nield, "The boundary correction for the Rayleigh-Darcy problem: limitations of the Brnkman equation," *J. Fluid Mech.* **128**, 37-46 (1983).

[12] J. Rubinstein, "Effective equations for flow in random porous media with a large number of scales," *J. Fluid Mech.* **170**, 379-383 (1986).

[13] L. Durlofsky and J. F. Brady, "Analysis of the Brinkman equation as a model for flow in porous media," *Phys. Fluids* **30**, 3329-3341 (1987).

[14] K. Vafai and S. J. Kim, "Fluid mechanics of the interface region between a porous medium and a fluid layer-an exact solution," *Int. J. Heat Fluid Flow* **11**, 254-256 (1990).

[15] D. A. Nield, "The limitations of the Brinkman-Forchheimer equation in modeling flow in a saturated porous medium and at an interface," *Int. J. Heat Fluid Flow* **12**, 269-272 (1991).

[16] K. Vafai and S. J. Kim, "On the limitations of the Brinkman-Forchheimer-extended Darcy equation," *Int. J. Heat Fluid Flow* **16**, 11-15 (1995).

[17] D. F. James and A. M. J. Davis, "Flow at the interface of a model fibrous porous medium," *J. Fluid Mech.* **426**, 47-72 (2001).

[18] B, Goyeau, D. Lhuillier, D. Gobin and M. G. Velarde, "Momentum transport at a fluid-porous interface," *Int. J. Heat Mass Transfer* **46**, 4071-4081 (2003).

[19] P. Mirbod, Z. Wu and G. Ahmadi, "Laminar flow drag reduction on soft porous media,"

Sci. Rep. **7**, 17263 (2017).

[20] M. Quintard and S. Whitaker, "Transport in ordered and disordered porous media. □: generalized volume averaging," *Transport Porous Med.* **14**, 179-206 (1994).

[21] S. Whitaker, "The Forchheimer equation: a theoretical development," *Transport Porous Med.* **25**, 27-61 (1996).

[22] R. D. Blevins, *Applied fluid dynamics handbook*, New York, Van Nostrand Reinhold Co. (1984).

[23] I. Battiato, "Self-similarity in coupled Brinkman/Navier-Stokes flows," *J. Fluid Mech.* **699**, 94-114 (2012).

[24] Z. Wu and P. Mirbod, "Experimental analysis of the flow near the boundary of random porous media," *Phys. Fluids* **30**, 047103 (2018).

[25] J. A. Ochoa-Tapia, "Momentum transfer at the boundary between a porous medium and a homogeneous fluid□□. Comparison with experiment," *Int. J. Heat Mass Transfer* **38**, 2647-2655 (1995).

[26] C. Beckermann, R. Viskanta and S. Ramadhyani, "Natural convection in vertical enclosures containing simultaneously fluid and porous layers," *J. Fluid Mech.* **186**, 257-284 (1988).

[27] W. P. Breugem and B. J. Boersma, "Direct numerical simulations of turbulent flow over a permeable wall using a direct and continuum approach," *Phys. Fluids* **17**, 025103 (2005).

[28] M. Chandesris, A. D'Hueppe, B. Mathieu, D. Jamet and B. Goyeau, "Direct numerical simulation of turbulent heat transfer in a fluid-porous domain," *Phys. Fluids* **25**, 125110 (2013).

[29] M. E. Rosti, L. Cortelezzi and M. Quadrio, "Direct numerical simulation of turbulent channel flow over porous walls," *J. Fluid Mech.* **784**, 396-442 (2015).

[30] C. Kang and K.-S. Yang, "Heat transfer characteristics of baffled channel flow," *ASME J. Heat Transfer* **133**, 091901 (2011).

[31] C. Kang and K.-S. Yang, "Flow instability in baffled channel flow," *Int. J. Heat Fluid Flow* **38**, 40-49 (2012).

[32] J. Kim and P. Moin, "Application of a fractional-step method to incompressible Navier-Stokes equations," *J. Comp. Phys.* **59**, 308-323 (1985).

[33] H. M. Nepf, "Flow and transport in regions with aquatic vegetation," *Annu. Rev. Fluid Mech.* **44**, 123-142 (2012).

[34] Q. Wu, Y. Andreopoulos and S. Weinbaum, "From red cells to snowboarding: A new

concept for a train track," *Phys. Rev. Lett.* **93**, 194501 (2004).

[35] P. Mirbod, Y. Andreopoulos and S. Weinbaum, "On the generation of lift forces in random soft porous media," *J. Fluid Mech.* **619**, 147-166 (2009).

[36] P. Mirbod, Y. Andreopoulos and S. Weinbaum, "Application of soft porous materials to a high-speed train track," *J. Por. Media* **12**, 1037-1052 (2009).

[37] C. Zhang, Z. Deng and Y. Chen, "Temperature jump at rough gas-solid interface in Couette flow with a rough surface described by Cantor fractal," *Int. J. Heat Mass Transfer* **70**, 322-329 (2014).

[38] H. Yan, W.-M. Zhang and Z.-K. Peng, "Effect of random surface topography on the gaseous flow in microtubes with an extended slip model," *Microfluid Nanofluid* **18**, 897-910 (2015).

[39] L. Bao, N. V. Priezjev, H. Hu and K. Luo, "Effects of viscous heating and wall-fluid interaction energy on rate-dependent slip behavior of simple fluids," *Phys. Rev. E* **96**, 033110 (2017).

[40] P. Mirbod, "Two-dimensional computational fluid dynamical investigation of particle migration in rotating eccentric cylinders using suspension balance model," *Int. J. Multiphase Flow* **80**, 79-88 (2016).

[41] P. Mirbod, "Analytical model of the feto-placental vascular system: consideration of placental oxygen transport," *R. Soc. open sci.* **5**, 180219 (2018).